Nonadiabatic theory of strong-field atomic effects under elliptical polarization

Xu Wang and J. H. Eberly

Nonadiabatic theory of strong-field atomic effects under elliptical polarization

Xu Wang and J. H. Eberly
Rochester Theory Center and the Department of Physics and Astronomy, University of Rochester, Rochester, New York 14627, USA

Elliptically polarized laser fields provide a new channel for access to strong-field processes that are either suppressed or not present under linear polarization. Quantum theory is mostly unavailable for their analysis, and we report here results of a systematic study based on a classical ensemble theory with solution of the relevant *ab inito* time-dependent Newton equations for selected model atoms. The study's approach is necessarily nonadiabatic, as it follows individual electron trajectories leading to single, double, and triple ionizations. Of particular interest are new results bearing on open questions concerning experimental reports of unexplained species dependences as well as double-electron release times that are badly matched by a conventional adiabatic quantum tunneling theory. We also report the first analysis of electron trajectories for sequential and non-sequential triple ionization. © 2012 American Institute of Physics. [http://dx.doi.org/10.1063/1.4752079]

I. INTRODUCTION

The interaction between intense laser fields and gas phase atoms or molecules has been studied extensively during the recent past. Many new physical processes have been observed, such as multiphoton ionization,[1] above-threshold ionization,[2] high harmonic generation,[3] nonsequential double ionization (NSDI),[4,5] attosecond pulse generation,[6] etc.

For accurate understanding of these processes, electron motion must be followed closely in all cases. However, many of these phenomena can be understood heuristically by a three-step recollision scenario.[7] An illustration is shown in Fig. 1. First, an electron is emitted via tunneling through the laser-tilted Coulomb barrier[8] and driven away by the laser field (left panel); second, this electron can be driven back to recollide with its parent ion when the laser field reverses its direction (middle panel); third, on recollision, several physical processes are possible: the recolliding electron can kick out a second electron leading to double ionization (right panel), or it can be recaptured by the ion core leading to the emission of a high harmonic photon, or it can be accelerated via elastic scattering.

We note that the initial step, when considered to occur via tunneling, has an obvious quantum origin and a clear visualization. The well-known tunneling rate expresses the ability of the electron orbital's standing wavefunction to gradually emerge through the Coulomb barrier, in a sense averaged over many electron bounces against the barrier from inside. This familiar adiabatically smoothed scenario is being challenged by new experimental data,[9] obtained from atomic double ionization of argon initiated by elliptically polarized light. The measured emission times for the two electrons deviate from the predictions of a tunneling theory, implying the potential role for nonadiabatic effects, and this is one of the questions we address. Another question to which elliptical polarization provides new access is species dependence of atomic behavior in high fields. Different atoms or molecules react quite differently to laser field ellipticity.[10–14] Calculations for double ionization under elliptical polarization with two different model atomic species and under different conditions are reported.

II. WHAT KIND OF THEORY?

Classical theories have been used to obtain insights for ionization via elliptical and circular polarization and some new understanding has been achieved in this way.[15–19] Although one would obviously prefer a quantum treatment, the various time-dependent Schrödinger equations for general quantum systems do not have analytical solutions. Worse, they do not even admit satisfactory numerical solutions. Consider the facts. After being released, an electron can travel a relatively large distance (∼1000 a.u.) in the laser field before the end of the pulse. On the other hand, the details within the atom are of the size ∼1 a.u. In terms of a grid for integration, for each spatial dimension, about 1000 grid points are needed. For a two-electron system, the total dimension is 6, so the total number of grid points needed is $(1000)^6 = 10^{18}$. This means a computer memory of 1 million terabytes just to store each time step! What is even worse is propagation over the entire pulse, usually composed of over 1000 time steps.

The only available non-perturbative answer to these difficult restrictions lies in classical modeling. Even for non-perturbatively strong fields and elliptical polarization, the nonadiabatic and fully *ab initio* integration of the classical time-dependent Newtonian equations (TDNE) is numerically trivial.

The general idea of the classical ensemble method is to mimic the multielectronic quantum wavefunction with an ensemble of classically modeled atoms. No quantum wave feature is included, such as quantum tunneling or interference, etc. The laser field is also modeled classically. The motion of electrons is determined by numerically integrating the classical TDNE. The classical ensemble method has been explained
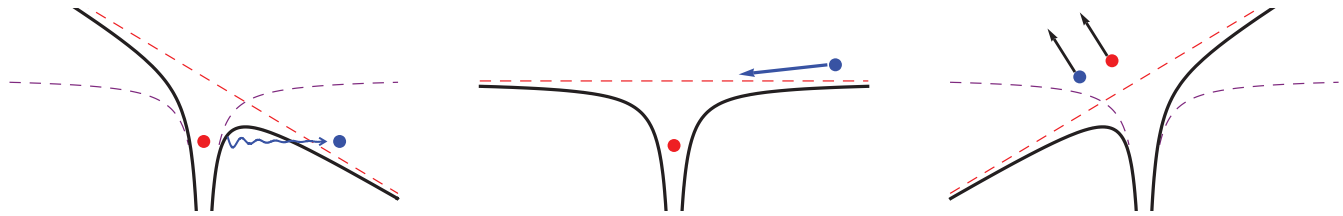
FIG. 1. Illustration of the three-step recollision model. Left: an electron is emitted via tunneling through the laser-titled Coulomb barrier; Middle: this electron can be driven back when the laser field reverses its direction; Right: the returning electron kicks out a second electron, leading to correlated double ionization.

in detail in Ref. 20, and its contribution to strong-field atomic ionization has been well-known.[21–27] Here we only give a brief introduction to it.

The first step is to generate a microcanonical ensemble of classically modeled atoms.[28,29] In this paper, the model atom is generated with two (for single and double ionization) or three (for triple ionization) active electrons. The ensemble is generated such that the total energy (E_{tot}) is fixed for each ensemble member (i.e., each model atom),

$$E_{tot} = \sum_{i=1}^{N} \left(\frac{p_i^2}{2} - \frac{N}{\sqrt{r_i^2 + a^2}} \right) + \sum_{i<j} \frac{1}{\sqrt{r_{ij}^2 + b^2}}, \quad (1)$$

where N is the number of electrons, p_i and r_i are the momentum and position of the ith electron, and r_{ij} is the distance between the ith and the jth electrons. Atomic units are used. Note that the Coulomb potential has been softened[30,31] with parameter a between the ion core and the electrons and with parameter b between the electrons.

To take account of species dependency, two atom models will be used. One is a model Ar atom, with energy $E_{tot} = -1.6$ a.u.; the other is a model "Xe/Kr" atom, with energy $E_{tot} = -1.3$ a.u.[32] Given the total energy, the positions and momenta of electrons are randomly assigned. We will show that the model Ar atom and the model Xe/Kr atom are surprisingly different when subject to double ionization with elliptical or circular polarization: for Ar, almost no recollisions occur and double ionization is not possible with elliptical polarization, and for Xe/Kr, recollision and double ionization are noticeable even with circular polarization.

The parameter a used in Eq. (1) is determined by the value of E_{tot}: given a value of E_{tot}, the parameter a is usually confined to a narrow range of about $\Delta a \sim 0.1$ a.u. For the model Ar atom, we choose a to be 1.5 a.u. For the model Xe/Kr atom, we choose a to be 1.8 a.u. The parameter b is not relevant to the stabilization of the model atom. It is set to be 0.1 a.u. only for the purpose of avoiding numerical singularities that may cause problems during calculation.

After the ensemble is prepared, an elliptically polarized laser pulse is turned on. For the intensities considered in this paper, which are on the order of 1 PW/cm², relativistic effects are small and the magnetic part of the laser field can be neglected. The laser electric field can be expressed as

$$\vec{E}_L(t) = E_0 f(t) \left[\hat{x} \sin(\omega t + \phi) + \hat{y} \varepsilon \cos(\omega t + \phi) \right], \quad (2)$$

where E_0 is the peak amplitude, ω is the angular frequency, ε is the ellipticity value, ϕ is the carrier-envelope phase, and $f(t)$ is the pulse envelope function. Most of the strong-field

experiments have been done with non-stabilized phase so in our simulation each model atom is assigned a pulse with a random ϕ value within $(0, 2\pi)$.

Figure 2 shows a sine-squared pulse with ellipticity value 0.5. The red curve shows the field along the major polarization direction and the blue curve shows the field along the minor polarization direction. Due to ellipticity, the amplitude of the blue curve is smaller than that of the red curve. (This obvious point will turn out to be important.) And there is a $\pi/2$ phase difference between the two curves.

The electrons undergo field-free interactions until the laser pulse is turned on. Then the motion of the electrons is governed by the TDNEs

$$\frac{d\vec{r}}{dt} = \frac{\partial H}{\partial \vec{p}}, \quad \frac{d\vec{p}}{dt} = -\frac{\partial H}{\partial \vec{r}}, \quad (3)$$

where the Hamiltonian, including the time-dependent laser interaction, is

$$H = H(t) = E_{tot} + \sum_{i=1}^{N} [x_i E_x(t) + y_i E_y(t)]. \quad (4)$$

The TDNEs are integrated numerically from the beginning to the end of the pulse. The laser field is given the common experimental wavelength $\lambda = 780$ nm ($\omega = 0.0584$ a.u.). The positions and momenta of electrons are recorded at each time step until the end of the pulse. At the end of the pulse, an ionization criterion will be applied to check the final ionization status. Our criterion defines an electron to be ionized if its distance to the ion core is larger than 6 a.u. A slight difference in this critical distance will not affect our discussions and conclusions in this paper. Depending on the number of ionized electrons, a model atom will fall into one of four possible categories, namely, no ionization, single ionization, double ionization, and triple ionization.
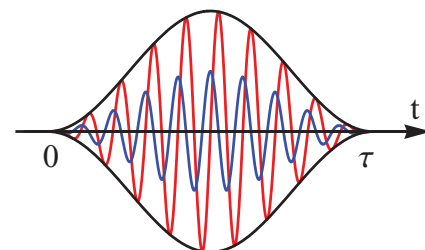

FIG. 2. An elliptically polarized pulse with ellipticity value 0.5. The red curve is the field along the major polarization direction and the blue curve is the field along the minor polarization direction.
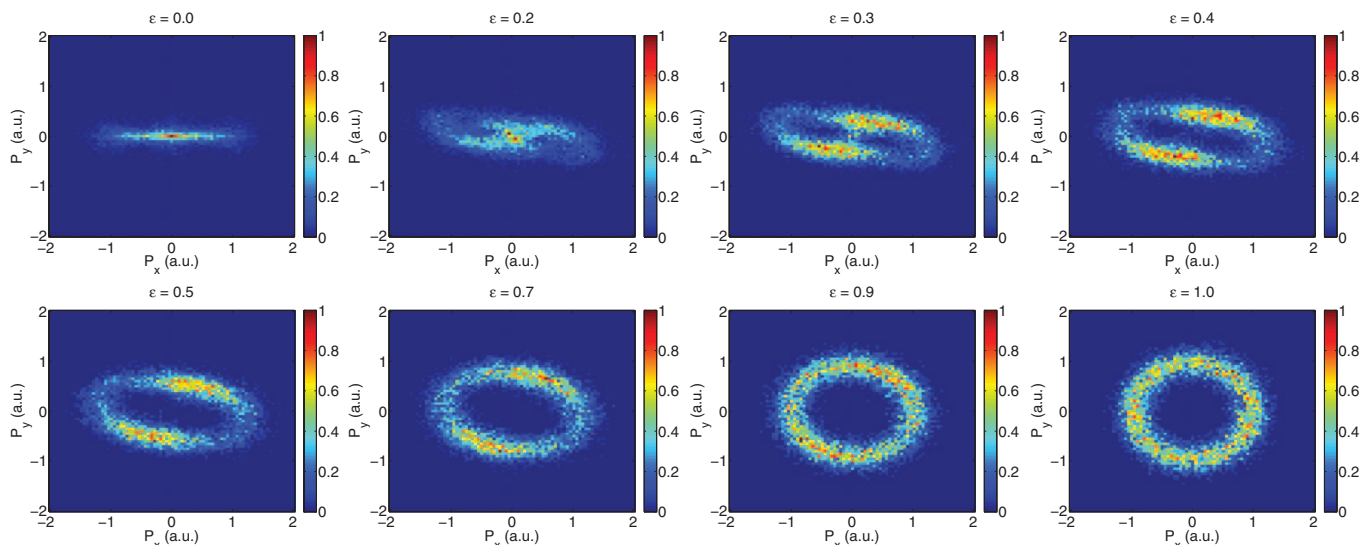
FIG. 3. Momentum distributions of single ionization for ellipticity from 0 (linear polarization) to 1 (circular polarization). Ellipticity values are labeled at the top of each figure. These distributions are obtained using the Ar model atom with intensity 1 PW/cm^2.

III. SINGLE IONIZATION

We will start from single ionization. Even this simple situation presents questions that are still open. The model Ar atom has been used for our TDNE calculations and subjected to a peak intensity of 1 PW/cm^2 for ellipticity values from linear to elliptical to circular. At the end of the pulse, single ionization events are collected and the ion momentum distributions on the polarization plane (i.e., the x-y plane) are plotted, as in Fig. 3, for a wide range of ellipticity values from 0 (linear polarization) to 1 (circular polarization). One sees that for linear polarization, the momentum distribution mainly aligns along the major polarization direction (i.e., the x direction) and peaks at $P_x = 0$. As ellipticity increases, it gradually splits into two parts along the minor polarization direction (i.e., the y direction). The distribution has an elliptical shape for mid-ellipticity values, although the population is not evenly distributed: the first and the third quadrants are denser than the second and the fourth quadrants. As the ellipticity value increases to 1.0, the distribution becomes circularly symmetric, as would be expected.

The consequences of elliptical polarization can be seen more clearly by projecting the 2D distributions onto individual axes. For example, Fig. 4 shows the projections for ellipticity 0.5. The distribution along the x direction is still peaked

at zero, similar to the situation of linear polarization, whereas the distribution along the y direction shows a two-peak structure with a minimum at zero. The two-peak structure along the y direction is, of course, not available with linear polarization. We have already shown[33] that it conveys important information about the ionization process, such as the ionization time itself, and about the target atom.

An open question is nearly hidden in Fig. 3 for mid-range ellipticities. Inspection shows that the uneven distribution mentioned above causes a distinct tilt of the ion cloud axis, pointing approximately to 1 o'clock rather than straight up. This has been tentatively identified as a deviation from the so-called Simpleman theory,[34] in which the electron responds only to the laser field. That is, ellipticity has allowed a contribution by the Coulomb field of the ion to make its first appearance. A theory of this axis tilt is of current interest.[35]

IV. DOUBLE IONIZATION AND NONADIABATIC ELECTRON RELEASE

Double ionization can be roughly divided into two categories, namely, sequential double ionization (SDI) and nonsequential double ionization (NSDI), depending on whether recollision is involved. Without recollision, the ionization of the two electrons can be viewed as independent without noticeable e-e correlations. With recollision, the two electrons cannot be viewed as independent and there are some recollision-imposed correlations between the two electrons. We will start in this section from the simpler case of SDI, and then NSDI will be discussed later.

The momentum distributions of doubly charged ions are shown in Fig. 5 and they can be compared to the single-electron distributions in Fig. 3. The distribution for linear polarization is again aligned along the x direction. As ellipticity increases to 0.1, it separates into two parts along the y direction. As ellipticity increases to 0.3, each of the two parts further separates into two new parts, leading to a four-band
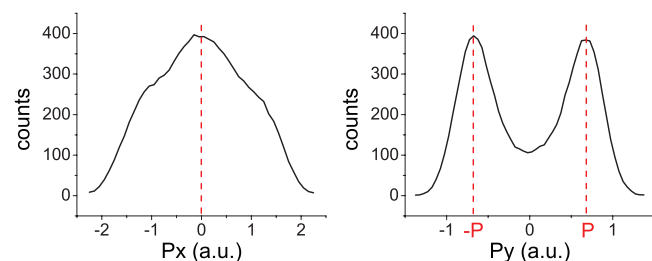

FIG. 4. Projection of the 2D momentum distribution with ellipticity value 0.5 (see Fig. 3, 2nd row, 1st panel) onto the major direction (left) and onto the minor direction (right).
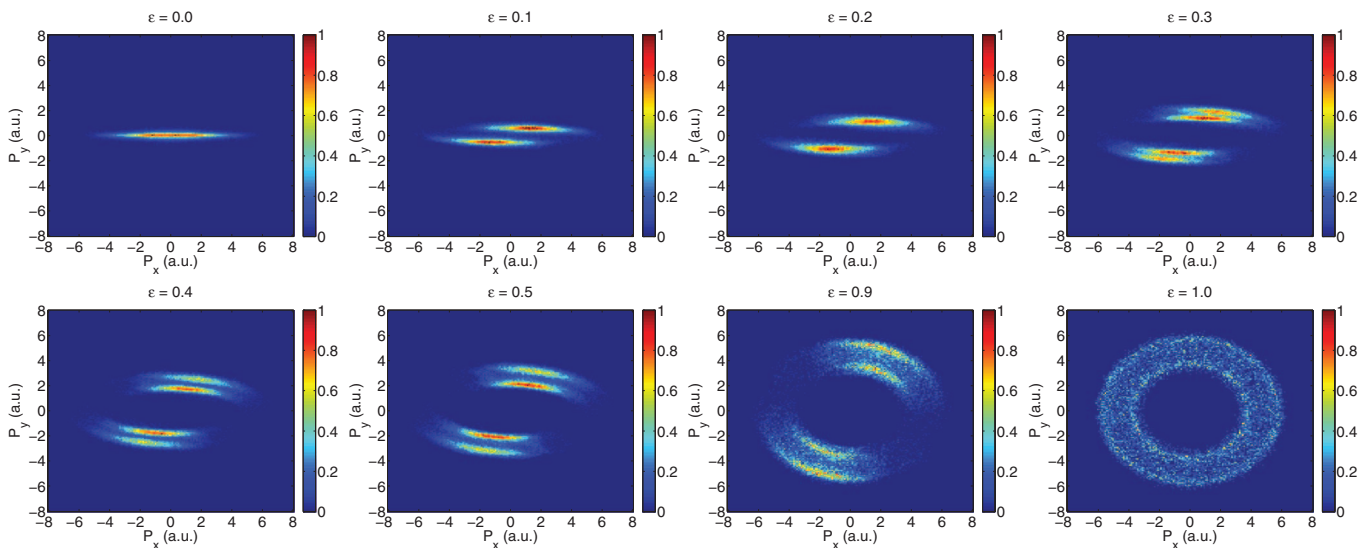
FIG. 5. Momentum distributions of doubly charged ions with various ellipticities from 0 to 1. Ellipticity values are labeled at the top of each panel. These distributions are obtained using the Ar model atom with intensity 3 PW/cm^2.

structure which can be seen more clearly above ellipticity 0.4. The main features of the four-band structure are preserved up to ellipticity 0.9. For circular polarization, the distribution becomes circularly symmetric.

The nature of the four-band structure can be seen more clearly by projecting the 2D momentum distributions onto individual axes. For example, Fig. 6 shows the two projections for ellipticity 0.5. The distribution shows a normal broad single peak structure centered at zero along the x direction, as in the situation of linear polarization. What is interesting is the projection along the y direction, which shows a four-peak structure, corresponding to the four bands in the 2D distribution. A full discussion is given in Ref. 33.

The physical meaning of the four-peak structure can be seen more clearly from Fig. 7, which shows two classes of SDI electron trajectories. The left panel shows the situation that both electrons are emitted to the same direction (the +x direction here) and the right panel shows the situation that the two electrons are emitted to opposite directions (one to +x and the other to −x). If both electrons are emitted to the same direction (both to +x or to −x), they will be twisted up or down by the laser field to the same y direction and end up with p_{1y} and p_{2y} of the same sign, so the resultant doubly charged ion is more likely to have a large net momentum along the y

direction. This corresponds to the outer two peaks of the four-peak structure. If the two electrons are emitted to opposite directions (one to +x and the other to −x), the two electrons will then be twisted up or down to opposite y directions, so the resultant doubly charged ion is more likely to have a small net momentum along the y direction. This corresponds to the inner two peaks of the four-peak structure.

Recently Pfeiffer *et al.* took advantage of the information provided by elliptical polarization and measured the electron emission times from argon in SDI.[9] The experimental data were compared to the predictions of an adiabatic tunneling theory[36] based on an independent-electron or single-active-electron (SAE) approximation. Figure 8 shows that although the emission time of the first electron agrees well with the adiabatic tunneling theory, the emission time of the second electron is substantially earlier than the prediction.

Conjectures have been made about explanations for the discrepancy of the second electron emission time between the adiabatic tunneling theory and the experiment. Zhou *et al.*[37] successfully reproduced the experiment using a classical TDNE approach that takes into account full e-e correlations. Thus it is natural to suspect that e-e correlations, which
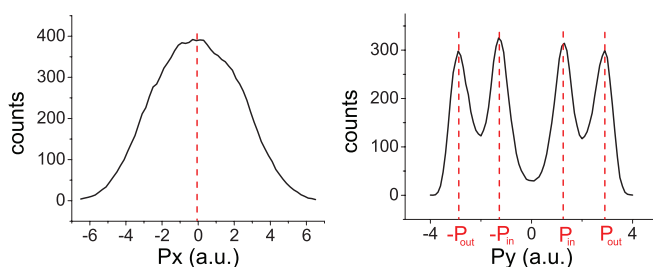

FIG. 6. Projection of the 2D momentum distribution with ellipticity value 0.5 (see Fig. 5, 2nd row, 2nd panel) onto the major direction (left) and onto the minor direction (right).
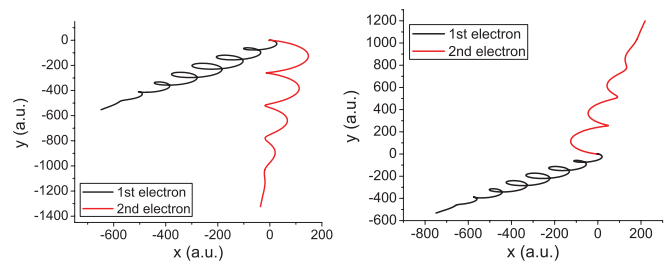

FIG. 7. Two typical SDI electron trajectories with ellipticity 0.5. The left panel demonstrates the situation that both electrons are emitted to the same direction (+x direction here), corresponding to the outer two peaks of the four-peak structure; The right panel demonstrates the situation that the two electrons are emitted to opposite directions (one to +x and the other to −x), corresponding to the inner two peaks of the four-peak structure.
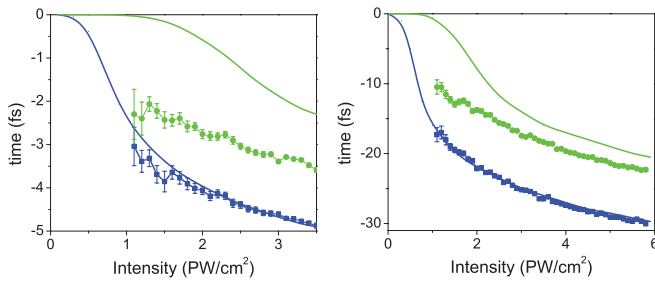
FIG. 8. Comparison of the predictions of the adiabatic tunneling theory (solid lines) of emission times with experiment (dots with error bars). The left panel is for pulse duration of 7 fs and the right panel is for 33 fs. Blue color is for first ionization and green color is for second ionization. Adapted from Ref. 9.
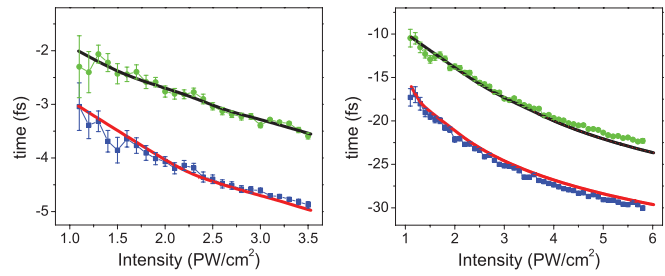

FIG. 9. Comparison of TDNE predictions of emission times with experiment, obtained with the SAE-based classical calculations, as explained in the text. The left panel is for the 7 fs pulse and the right panel is for the 33 fs pulse. Dots with error bars are the experimental data adapted from Ref. 9. Lower and upper solid lines are the classical SAE predictions of the 1st and the 2nd ionization, respectively.

are not included in a SAE-based adiabatic tunneling theory, play an important role. However, the specific physical consequence of the e-e correlations is far from obvious at this time.

We note that an alternate conjecture is possible. It separates adiabaticity and the SAE approximation, and suggests that it is the adiabaticity assumption, instead of the SAE approximation, that breaks down. To test this idea, one needs a SAE-based but nonadiabatic theory for comparison. A natural option is an unconventional SAE-based classical approach, which is only slightly different from the traditional method described above and will be sketched below. We want to emphasize that the classical approach is intrinsically a nonadiabatic one: in the classical approach, an electron is removed by the laser field with an obvious finite velocity, but tunneling removal of an electron leaves it with near zero velocity on the exterior of the Coulomb well.

Our new SAE-based classical approach follows exactly the SAE prescription: initially there is only one electron in the model atom, the energy of which is set to be the negative of the first ionization potential of Ar (the target used in the experiment),

$$E_1 = \frac{\mathbf{p}_1^2}{2} - \frac{1}{\sqrt{\mathbf{r}_1^2 + 1}} \equiv -IP_1 = -0.6 \text{ a.u.} \quad (5)$$

The position and momentum are randomly assigned. Then the laser pulse is turned on. Only when this electron is driven away by the laser field, defined as a distance of 10 a.u. away from the ion core, does a second electron become active. In our approach, a second electron is "created" near the ion core with energy E_2, which can be written as

$$E_2 = \frac{\mathbf{p}_2^2}{2} - \frac{2}{\sqrt{\mathbf{r}_2^2 + 1}} \equiv -IP_2 = -1.0 \text{ a.u.} \quad (6)$$

The second electron reacts nonadiabatically to all the forces on it. These forces include the Coulomb attraction from the ion core, the laser electric force, and the repulsive force from the first electron, which is already negligibly weak. The motion of the second electron is also governed by the classical TDNE in the same way. If the laser field is strong enough, the second electron can be ionized.

The electron emission times obtained using the enforced-SAE nonadiabatic classical method are shown in Fig. 9, in

comparison with the experiment. As one sees, the calculation agrees quantitatively with the experiment throughout the entire intensity range, for both electrons.

The comparison of the SAE-based adiabatic tunneling theory and the SAE-based nonadiabatic classical theory with experiment strongly suggests that nonadiabatic effects play an important role in electron emission. Yet the specific physical mechanism remains an open question and requires further exploration.
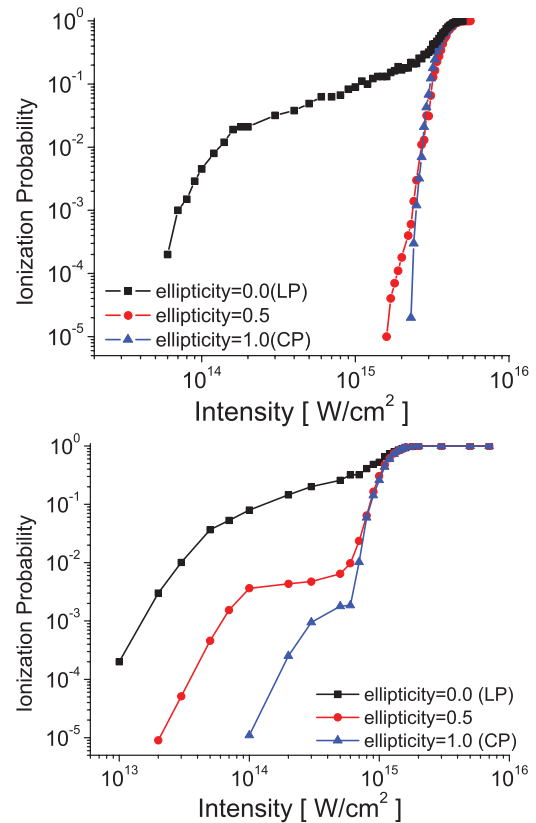

FIG. 10. Ionization probability obtained in numerical experiments as a function of laser peak intensity under different ellipticities for the model Ar atom (top) and the model Xe/Kr atom (bottom). For Ar, the knee is tiny but recognizable for ellipticity 0.5 and completely disappears for CP. For Xe/Kr, the knee remains noticeable even for CP. The bottom panel is adapted from New J. Phys. 12, 093047 (2010). Reproduced with permission of IOP Publishing Ltd and Deutsche Physikalische Gesellschaft. Copyright 2010 IOP Publishing Ltd and Deutsche Physikalische Gesellschaft.
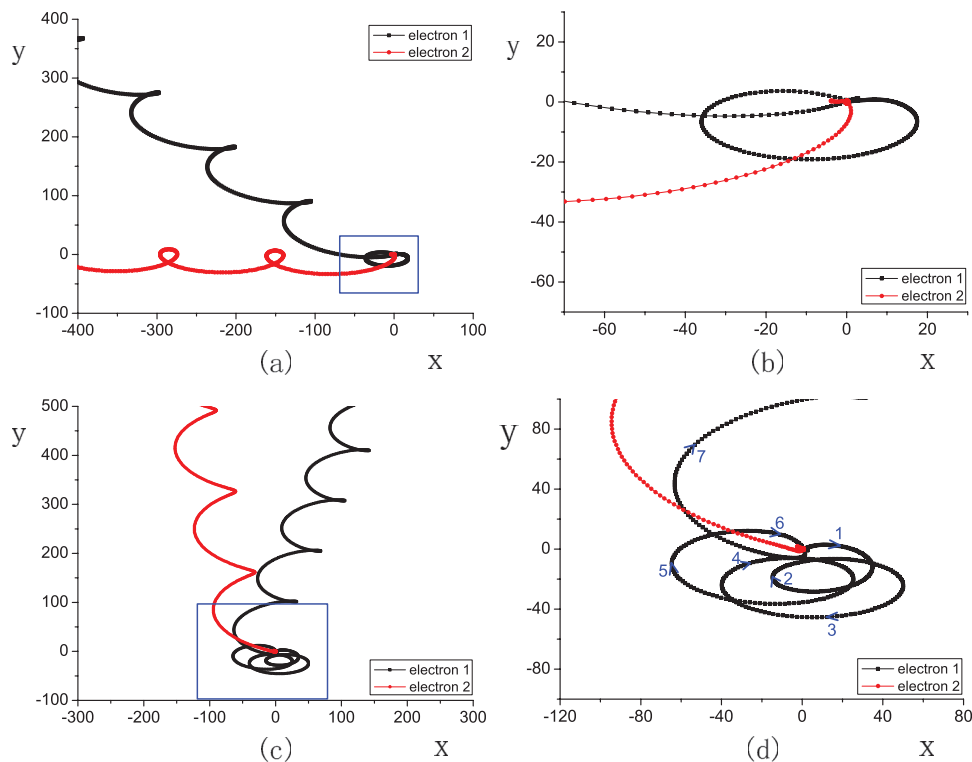
FIG. 11. Two typical recollision trajectories for ellipticity 0.5. The blue boxes of the left two figures are greatly expanded to give the right two figures. Top: the recolliding electron's trajectory is an almost perfect ellipse. It returns to the origin in one laser cycle and kicks out the second electron. Bottom: the elliptical trajectory of the recolliding electron is distorted by the ion's Coulomb force and executes several cycles before coming close enough to the ion core to kick out the second electron. The arrows and numbers are used to show the temporal motion of the first electron. Adapted from New J. Phys. 12, 093047 (2010). Reproduced with permission of IOP Publishing Ltd and Deutsche Physikalische Gesellschaft. Copyright 2010 IOP Publishing Ltd and Deutsche Physikalische Gesellschaft.

V. SPECIES DEPENDENCES UNDER ELLIPTICAL POLARIZATION

Nonsequential double ionization shows up in the ionization-probability-versus-intensity plot as a so-called "knee" structure,[4,5] which has been widely used as a signature of recollision and NSDI. Experiments have tested the persistency of the knee when subjected to elliptical and circular polarization. The results show a clear species dependence: for some atoms, such as Ne and Ar, the knee drops quickly and disappears as ellipticity increases;[10,11] for some other atoms or molecules, such as NO,[12] O_2,[13] and Mg,[14] the knee persists even with circular polarization.
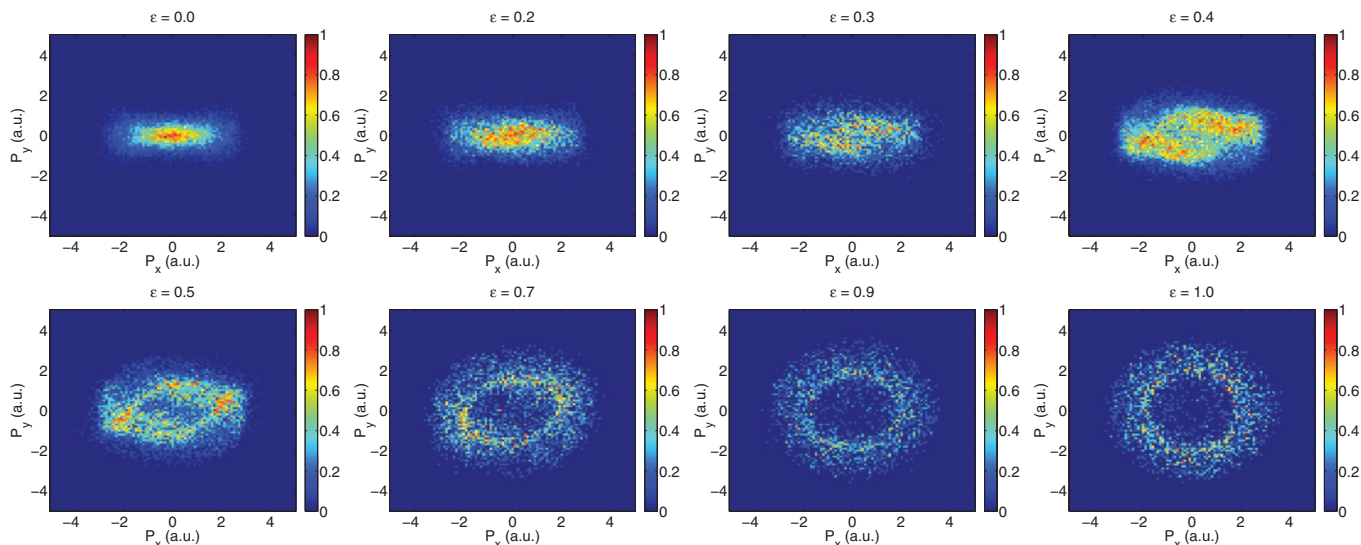

FIG. 12. Momentum distributions of NSDI with various ellipticities from 0 to 1. Ellipticity values are labeled at the top of each panel. These distributions are obtained using the Xe/Kr model atom with intensity 0.5 PW/cm^2.
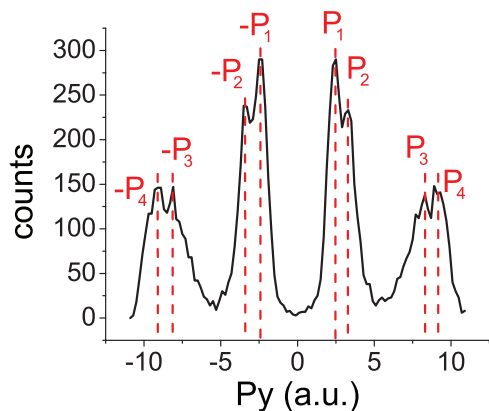
FIG. 13. Momentum distribution of triply charged ions along the y direction for ellipticity 0.5. Eight peaks can be recognized although separations between the two-peak pairs is small. Laser peak intensity is 30 PW/cm^2.

These experimental findings are largely unsupported by prior theoretical study, but we can now report that in classical TDNE calculations under elliptical polarization, recollision and NSDI also show a strong species dependency. Figure 10 shows the double ionization probability as a function of intensity for the model Ar atom (top) and the model Xe/Kr atom (bottom) at three different ellipticity values, namely, linear polarization, ellipticity 0.5, and circular polarization. In both cases, a strong knee shows up for linear

polarization. For Ar, the knee shrinks to a tiny but still recognizable one for ellipticity 0.5, and completely disappears for circular polarization. For Xe/Kr, the knee persists even with circular polarization. The occurrence or the non-occurrence of NSDI depends critically on the ionization energy (i.e., species) and the laser wavelength, and an interesting two-dimensional phase diagram is reported recently by Fu *et al.*, for a variety of atomic species and wavelengths.[38]

To understand NSDI with elliptical polarization we have back-analyzed successful NSDI events to determine the sequence of events that lead to a NSDI conclusion. If a particular outcome category is of interest (e.g., NSDI here), ensemble members that fall into this category at the pulse end will be picked up and their history during the pulse will be traced back. Back-analysis of classical trajectories is a very powerful tool to investigate detailed physical processes[39] and a quantum analog using wavefunction masking has also been developed by Haan *et al.*[40]

The surprising conclusion of this back analysis is that every successful NSDI trajectory is elliptical. That is, in all cases examined, the first ionized electron circulates along an elliptical trajectory for one or more cycles and then collides and ejects the second electron. Typical trajectories showing one-cycle and multi-cycle ellipses are given in Fig. 11.

The momentum distribution of doubly charged ions induced by elliptical recollision trajectories is shown in Fig. 12, for various ellipticities from 0 to 1. These distributions are
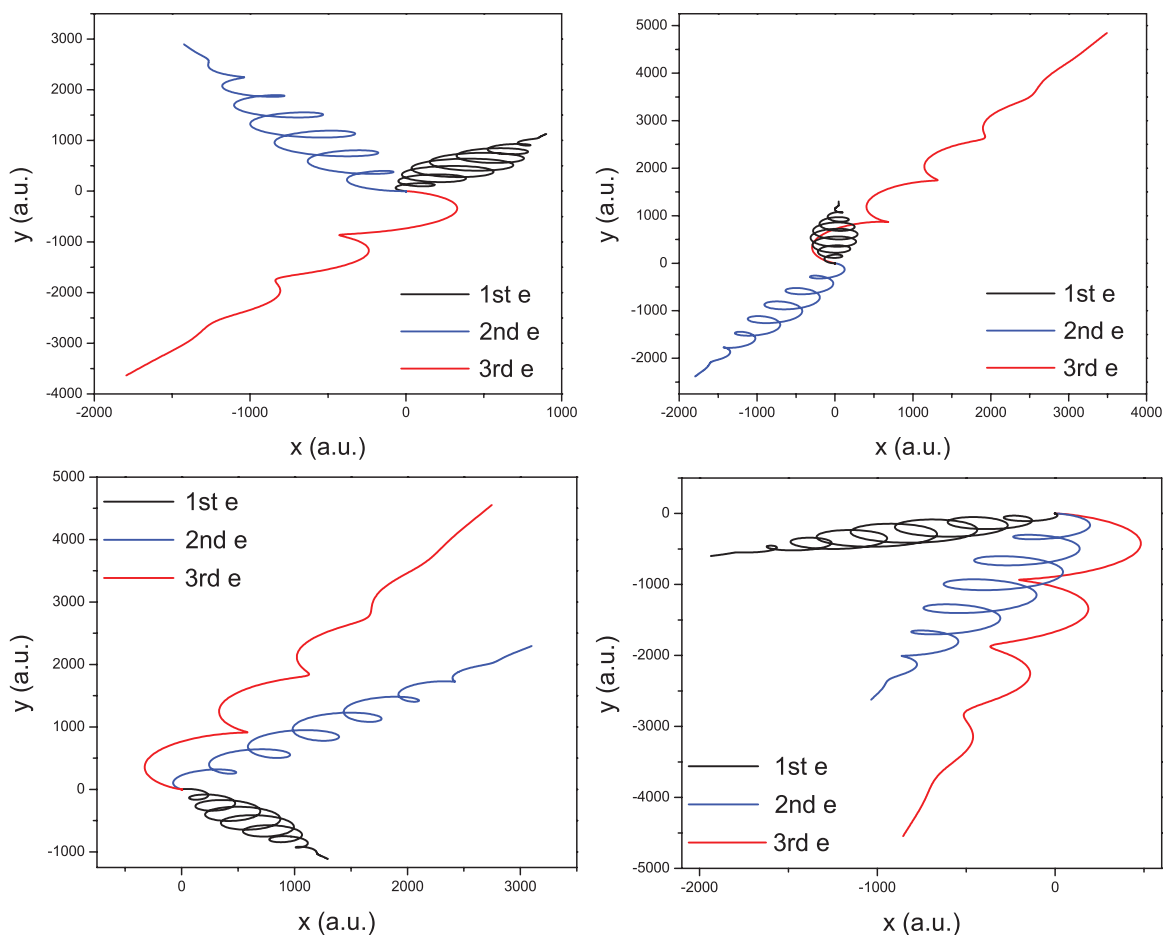

FIG. 14. Four typical STI trajectories, corresponding to momentum peaks P_1, P_2, P_3, and P_4 of Fig. 13, respectively.

obtained using the Xe/Kr model atom at intensity 0.5 PW/cm^2. From the knee figure shown in the second panel of Fig. 10, this intensity is within the knee region for all ellipticity values, so all double ionizations obtained are recollision-induced NSDI.

Except for near-linear or near-circular polarization, the ion momentum distribution in Fig. 12 of NSDI with elliptical polarization looks completely different from that of SDI in Fig. 5. The four-peak feature shown in SDI disappears, and is replaced by a "mouth-shape" structure. So SDI and NSDI leave different traces on the momentum plane and this difference can be used to tell which ionization channel has been followed.

We point out that the existence of the elliptical trajectories has not been confirmed by experiment, although we propose them as a possible mechanism to explain the experimentally observed knee structures shown in NO,[12] O$_2$,[13] and Mg.[14] These experiments were done before the COLTRIMS (COLd Target Recoil Ion Momentum Spectroscopy) technique[41] was widely adopted, so no momentum distribution data like those shown in Fig. 12 are available so far. It is thus desirable experimentally to measure the momentum distribution of the above targets with mid-elliptical polarization to see whether similar structures can be recovered.

VI. TRIPLE IONIZATION

Triple ionization is more complicated than double ionization because of the additional electron, and allows additional scenarios for electron release. It has not yet been studied systematically, but the physical dynamics is not essentially different. We report here that triple ionization can also be divided into two main categories, sequential triple ionization (STI) if the three electrons are ionized independently without recollision-induced correlations, and nonsequential triple ionization (NSTI) if recollision is important. For STI, similarly to single ionization and SDI, a multiple-peak structure will appear along the minor polarization direction and the number of peaks becomes 8 ($=2^3$). This Simpleman prediction of an eight-peak structure has been observed in our classical simulation, as shown in Fig. 13. Eight peaks can be recognized, although one of the spacings between neighboring peaks is small.

The physics of the eight-peak structure (four on each side) can be seen more clearly from Fig. 14, which shows four typical STI trajectories that correspond to the four different momentum peak values P_1, P_2, P_3, and P_4 as demonstrated in Fig. 13. Black, blue, and red colors show the trajectories of the 1st, 2nd, and 3rd electrons, respectively. The first panel shows the situation where the 1st electron and the 2nd electron are emitted to the same direction and the 3rd electron is emitted to the opposite direction, and this will lead to the least net momentum of the triply charged ion along the y direction, corresponding to the innermost two peaks ($\pm P_1$). The upper right panel shows the situation where the 1st electron and the 3rd electron are emitted to the same direction and the 2nd electron is emitted to the opposite direction, and this will lead to a larger net momentum of the ion along the y direction, corresponding to the $\pm P_2$ peaks. The lower left panel shows the
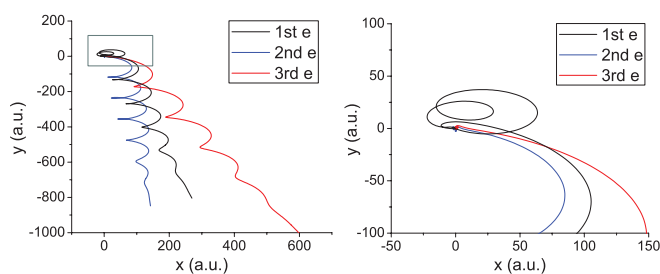

FIG. 15. An example of NSTI trajectory. The grey box in the left panel has been enlarged to give the right panel. The 1st electron oscillates along an elliptical trajectory for two cycles before kicking the remaining two electrons, leading to NSTI.

situation where the 2nd electron and the 3rd electron are emitted to the same direction and the 1st electron is emitted to the opposite direction, corresponding to the $\pm P_3$ peaks. The last panel shows the situation where all three electrons are emitted to the same direction, and this will lead to the largest net ion momentum along the y direction, corresponding to the two outermost peaks ($\pm P_4$).

Recollision is also possible via elliptical trajectories, leading to NSTI. An example is shown in Fig. 15, where the 1st emitted electron oscillates along an elliptical trajectory for two cycles and kicks out the other two electrons.

VII. SUMMARY

Atomic ionization with elliptical polarization has been systematically studied using the classical ensemble theory. The study covers a wide range of ionization channels including single ionization, sequential and nonsequential double ionization, and sequential and nonsequential triple ionization. Each ionization channel has been analyzed separately.

For the ionization channels that do not involve recollision (i.e., single ionization, SDI, and STI), the end-of-pulse ion momentum distributions, which can be measured experimentally using the COLTRIMS technique, are shown to have a multi-peak structure along the minor polarization direction. Singly charged ions show a two-peak structure, doubly charged ions show a four-peak structure, and triply charged ions show an eight-peak structure.

The positions of these peaks encode important ionization information that is not available with linear polarization. We show that the position of these peaks tells the ionization fields and the ionization times of emitted electrons: the momentum distribution of singly charged ions tells the ionization field and the ionization time of the emitted electron; the momentum distribution of doubly charged ions tells the ionization fields and the ionization times of both emitted electrons; and the momentum distribution of triply charged ions tells the ionization fields and the ionization times of all three emitted electrons.

The ionization fields and the ionization times of electrons have the promise of discovering new ionization dynamics, revealing new information about the target atom or molecule, and identifying new multielectron effects and nonadiabatic dynamics. A good example is the recent experiment by Pfeiffer et al.[9] measuring electron emission times in SDI. The

emission time of the second electron cannot be explained by the adiabatic tunneling theory while it can be reproduced by the nonadiabatic classical calculation. This strongly implies that nonadiabatic effects play an important role in atomic ionization.

For the ionization channels that involve recollision (i.e., NSDI and NSTI), we show that they are possible with elliptical and even circular polarization. Trajectory analysis shows that they occur via a new family of trajectories called by us elliptical trajectories. Elliptical trajectories are initiated if the first electron is emitted with a nonzero velocity along the minor direction and this velocity balances the laser-induced drift velocity. The probability of getting recollision can be much higher than normal expectation for some atomic or molecular species.

ACKNOWLEDGMENTS

[1]H. G. Muller, P. Agostini, and G. Petite, in *Atoms in Intense Laser Fields*, edited by M. Gavrila (Academic, 1992).

[2]P. Agostini, F. Fabre, G. Mainfray, G. Petite, and N. K. Rahman, Phys. Rev. Lett. **42**, 1127 (1979).

[3]A. L'Huillier, L. Lompré, G. Mainfray, and C. Manus, in *Atoms in Intense Laser Fields*, edited by M. Gavrila (Academic, 1992).

[4]D. N. Fittinghoff, P. R. Bolton, B. Chang, and K. C. Kulander, Phys. Rev. Lett. **69**, 2642 (1992).

[5]B. Walker, B. Sheehy, L. F. DiMauro, P. Agostini, K. J. Schafer, and K. C. Kulander, Phys. Rev. Lett. **73**, 1227 (1994).

[6]See the overview in F. Krausz and M. Ivanov, Rev. Mod. Phys. **81**, 163 (2009).

[7]P. B. Corkum, Phys. Rev. Lett. **71**, 1994 (1993).

[8]M. V. Ammosov, N. B. Delone, and V. P. Krainov, Zh. Eksp. Teor. Fiz. **91**, 2008 (1986).

[9]A. N. Pfeiffer, C. Cirelli, M. Smolarski, R. Dörner, and U. Keller, Nat. Phys. **7**, 428 (2011); see also commentary in K. Ueda and K. Ishikawa, Nat. Phys. **7**, 371 (2011).

[10]P. Dietrich, N. H. Burnett, M. Ivanov, and P. B. Corkum, Phys. Rev. A **50**, R3585 (1994).

[11]N. H. Burnett, C. Kan, and P. B. Corkum, Phys. Rev. A **51**, R3418 (1995).

[12]C. Guo and G. N. Gibson, Phys. Rev. A **63**, 040701(R) (2001).

[13]C. Guo, M. Li, J. P. Nibarger, and G. N. Gibson, Phys. Rev. A **58**, R4271 (1998).

[14]G. D. Gillen, M. A. Walker, and L. D. Van Woerkom, Phys. Rev. A **64**, 043413 (2001).

[15]N. I. Shvetsov-Shilovski, S. P. Goreslavski, S. V. Popruzhenko, and W. Becker, Phys. Rev. A **77**, 063405 (2008).

[16]X. Wang and J. H. Eberly, Phys. Rev. Lett. **103**, 103007 (2009).

[17]X. Wang and J. H. Eberly, New J. Phys. **12**, 093047 (2010).

[18]X. Wang and J. H. Eberly, Phys. Rev. Lett. **105**, 083001 (2010).

[19]F. Mauger, C. Chandre, and T. Uzer, Phys. Rev. Lett. **105**, 083002 (2010).

[20]R. Panfili, J. H. Eberly, and S. L. Haan, Opt. Express **8**, 431 (2001).

[21]P. J. Ho, R. Panfili, S. L. Haan, and J. H. Eberly, Phys. Rev. Lett. **94**, 093002 (2005).

[22]P. J. Ho and J. H. Eberly, Phys. Rev. Lett. **97**, 083001 (2006).

[23]P. J. Ho and J. H. Eberly, Opt. Express **15**, 1845 (2007).

[24]S. L. Haan, J. S. Van Dyke, and Z. S. Smith, Phys. Rev. Lett. **101**, 113001 (2008).

[25]S. L. Haan, Z. S. Smith, K. N. Shomsky, P. W. Plantinga, and T. L. Atallah, Phys. Rev. A **81**, 023409 (2010).

[26]F. Mauger, C. Chandre, and T. Uzer, Phys. Rev. Lett. **102**, 173002 (2009).

[27]F. Mauger, C. Chandre, and T. Uzer, Phys. Rev. Lett. **104**, 043005 (2010).

[28]R. Abrines and I. C. Percival, Proc. Phys. Soc. London **88**, 861 (1966).

[29]R. Abrines and I. C. Percival, Proc. Phys. Soc. London **88**, 873 (1966).

[30]J. Javanainen, J. H. Eberly, and Q. Su, Phys. Rev. A **38**, 3430 (1988).

[31]Q. Su and J. H. Eberly, Phys. Rev. A **44**, 5997 (1991).

[32]The energy of an atom is obtained by adding the first and the second ionization potentials of this atom. For Ar, this energy is $-(15.76\ \text{eV} + 27.63\ \text{eV})$ $= -43.39\ \text{eV} = -1.60$ a.u.; for Kr, this energy is -1.41 a.u. and for Xe, this energy is -1.23 a.u. The energy of the model Xe/Kr atom lies between Xe and Kr.

[33]X. Wang and J. H. Eberly, Phys. Rev. A **86**, 013421 (2012).

[34]The so-called Simpleman theory was defined and named by H. B. van Linden van den Heuvell and H. G. Muller, in *Multiphoton Processes*, edited by S. J. Smith and P. L. Knight (Cambridge University Press, 1988). It has been consistently useful for about 25 years.

[35]N. I. Shvetsov-Shilovski, D. Dimitrovski, and L. B. Madsen, Phys. Rev. A **85**, 023428 (2012).

[36]X. M. Tong and C. D. Lin, J. Phys. B **38**, 2593 (2005).

[37]Y. Zhou, C. Huang, Q. Liao, and P. Lu, Phys. Rev. Lett. **109**, 053004 (2012).

[38]L. B. Fu, G. G. Xin, D. F. Ye, and J. Liu, Phys. Rev. Lett. **108**, 103601 (2012).

[39]R. Panfili, S. L. Haan, and J. H. Eberly, Phys. Rev. Lett. **89**, 113001 (2002).

[40]S. L. Haan, P. S. Wheeler, R. Panfili and J. H. Eberly, Phys. Rev. A **66**, 061402(R) (2002).

[41]R. Dörner, V. Mergel, O. Jagutzki, L. Spielberger, J. Ullrich, R. Moshammer, and H. Schmidt-Böcking, Phys. Rep. **330**, 95 (2000).